Research Article

Investigating the Selective Control of Photoassociation of Yb$_2$

Junxia Cheng,[1] Bo Tian,[2] Siyu Li,[1] Jia Wang,[1] and Shenjiang Wu [1]

[1]*School of Photo-Electrical Engineering, Xi'an Technological University, Xi'an 710021, China*
[2]*College of Aerospace and Civil Engineering, Haerbin Engineering University, Haerbin 150001, China*

Correspondence should be addressed to Shenjiang Wu; 1225457175@qq.com

The selective control of photoassociation of Yb$_2$ is investigated in theory. Based on *ab initio* to rationalize Franck–Condon filtering, the optimal target states of photoassociation have been obtained. The corresponding vibrational transitions from X$^1\Sigma_g^+$ to the excited state (A$^1\Sigma_u^+$, B$^1\Pi_u$, C$^1\Sigma_u^+$, and D$^1\Pi_u$) are $v' = 23$, 50, 55, and 0, respectively. By using quantum wave packet dynamic methods, we calculated the yields with time evaluation for the selected target states. The projections of time-dependent wave functions of initial states on the target vibrational eigenstates reflected the synthetic yields of Yb$_2$. For target A$^1\Sigma_u^+$, we used Gaussian pulse to make the yield of $v' = 23$ up to 97% at 725 fs. After a laser pulse, the positive chirp promoted the yield of vibrational states to increase, but the negative chirp inhibited its decrease. For the D$^1\Pi_u$ state, when laser intensity is 1.0×10^{14} W/cm^2, the purity and yield of target state $v' = 0$ reached the maximum at 1350 fs. That is to say, changing the laser parameters and pulse shapes could control the photochemical reaction along our desired direction. These conditions will provide an important reference and suggest a scheme for a feasible photoassociation of further experimental and theoretical research studies. Current study may promote an important step toward the realization of highly accurate quantum manipulation and material synthesis.

1. Introduction

Optical atomic clocks [1, 2] have made it possible to test the fundamentals of physics [3] and place limits on temporal variation of fundamental constants [4–6], or to explore quantum many-body systems [7, 8], even to search for topological dark matter through its impact on the fine-structure constant [9, 10]. Meanwhile, molecular clocks promise increased sensitivity to the variation of the electron-to-proton mass ratio [11–15]. Laser cooling of spin-singlet atoms, such as calcium, strontium, or ytterbium, has gained widespread attention due to their possible applications in making nonmagnetic Bose-Einstein condensate, as well as atomic reference for optical clocks [16]. The effect of cold collisions is especially important for optical clocks with atoms trapped in one-dimensional optical lattices [17, 18]. Information about cold-collisional shifts may be obtained from molecular potentials [19, 20]. Directly photoassociative approach to measure $^1S_0 + {}^3P_0$ and $^3P_0 + {}^3P_0$ potentials may be challenging since nothing is known about bound state positions [21]. Additionally, Franck–Condon factors may be

unfavorable in case of ytterbium [15] which will make direct measurement even more challenging. Bober et al. reported an indirect photoassociative approach that may allow for determining the scattering lengths for $^1S_0 + {}^3P_0$ and $^3P_0 + {}^3P_0$ cold collisions using 679 nm laser [22].

Photoassociation (PA) is a process in which two colliding atoms form an excited molecule by absorbing a photon. This technique had been successfully applied to create ultracold molecules from ultracold atomic gases. Besides, ultracold atoms have also generated new avenues of research related to quantum physics, like Bose-Einstein condensation and atom optics. PA spectroscopy provides a versatile tool for probing the physics of rovibrational molecular states and precisely determining the collisional properties of atoms, such as scattering length and interatomic potential coefficients [23]. Furthermore, the PA process can be actively used to control the strength of atomic interaction via coupling to an excited molecular state. Schemes for internal rovibrational cooling in Yb$_2$ and Cd$_2$ based on photodissociation of $(^{171}$Yb)$_2$ are presented, which are based on exploration of the rotational and vibrational

energy structures using both theoretical and experimental approaches [24].

In addition, Borkowski et al. reported observations of photoassociative spectra near the intercombination line in isotopic mixtures of ultracold ytterbium gases. Several heteronuclear bound states have been found for the excited $^{170}Yb^{174}Yb$ and $^{174}Yb^{176}Yb$ molecules [16]. Roy et al. demonstrated interspecies collisions in a dual-species Yb–Li magnetooptical trap (MOT) and carried out PA spectroscopy of molecular potentials below the $Yb(^1S_0) + Li(^2P_{1/2})$ asymptote [25]. In theory, the potential energy curves of the ground and twelve low-lying excited electronic states of RbYb molecule have been calculated using the multireference perturbation theory method at the CASSCF/XMCQDPT2 level [26]. Some key theoretical predictions of the electronic structure and dipole moment of the ground and low-lying excited states of LiYb and the ground state of LiSr have recently been obtained [27].

In this work, we investigated the selective control of photoassociation of Yb_2 at short range that is organized as follows. In Section 2, the methods of *ab initio* calculations and wave packet dynamics for the allowed transitional states $(X^1\Sigma^+_g, A^1\Sigma_u^+, B^1\Pi_u, C^1\Sigma_u^+, D^1\Pi_u)$ of photoassociation are described. Section 3 includes the results and discussions of the data. Firstly, highly correlated *ab initio* calculations were performed for accurate determination of the potential energy curves (PECs) and transition dipole moment curves (TDMCs). Then, by Franck–Condon filtering, the optimal target states have provided a reliably photoassociative route for laser cooling. Finally, the yield and purity of photoassociation of Yb_2 molecule have been calculated by changing laser parameters and pulse shapes. Finally, the conclusions are made in Section 4.

2. Theory and Method of Calculations

2.1. Ab Initio Calculation. The *ab initio* calculations of electronic structure for the allowed transitional electronic states $(X^1\Sigma_g^+, A^1\Sigma_u^+, B^1\Pi_u, C^1\Sigma_u^+, D^1\Pi_u)$ of Yb_2 have been performed with MOLPRO [28] in the D_{2h} point group, where the symmetries of A_g, B_{3u}, B_{2u}, B_{1g}, B_{1u}, B_{2g}, B_{3g}, and A_u representations were used. The methods of complete active space self-consistent field (CASSCF) [29, 30] and internally contracted multireference configuration interaction plus Davidson corrections (icMRCI + Q) [31] have been adopted. For Yb atom, the basis set of effective core potential (ECP) ECP60MDF has been used [32]. We performed CASSCF and MRCI calculations with reference spaces consisting of 5s5p6s5d6p. The eight electrons in the 5s5p shells were put in the closed spaces, where it was doubly occupied in all reference configuration state but still optimized. For Yb_2 molecule, the active space of 4 electrons in 15 orbitals (6s, 6p, 5d) generates the appropriate reference wave functions. Thus, the corresponding active spaces are (32213220).

2.2. Wave Packet Dynamic Method. Combining with highly correlated *ab initio* calculations for accurate determination of the potential energy curves (PECs) and transition dipole moment curves (TDMCs), one could obtain the Franck–Condon factors and transitional probabilities. Using Franck–Condon filtering, vibrational coherence could be generated according to the maximum overlap [33]. The selected optimal target states have provided a feasible route for photoassociative process. Furthermore, the quantitative understanding of the yield and purity of target states after association has been studied by using quantum wave packet dynamic methods [34]. The projections of time-dependent wave functions of initial states on the vibrational eigenstates of excited states, reflecting the photoassociation yields, were investigate. The detailed calculation process can be found in our previous published article [35]. By changing the laser parameters and pulse shape, we studied the effects on yield and purity of photoassociation of Yb_2 molecule.

3. Results and Discussion

3.1. Potential Energies and Transition Dipole Moments of States. In 1, the potential energy curves (PECs) of Yb_2 molecule with a valid range $2.0 \leq R \leq 20$ Å have been presented, which included $X^1\Sigma_g^+$ and allowed transitions from ground to excited states $A^1\Sigma_u^+$, $B^1\Pi_u$, $C^1\Sigma_u^+$, and $D^1\Pi_u$. In order to estimate the accuracy of these various PECs over the range of R, we evaluated equilibrium internuclear distance (R_e), electronic transition energy (T_e), dissociation energy (D_e), harmonic frequency (ω_e), anharmonic vibrational frequency $(\omega_e x_e)$, and rotational frequency (B_e) of all states at icMRCI + Q/ECP60MDF/32213220 levels by LEVEL program [36]. There are few spectroscopic studies on this molecule. These produced spectroscopic constants of present results compared with the theoretical value [37, 38] that are also listed in Table 1 together. It can be seen that our results are in good agreement with the calculated results. Furthermore, there are much closer determinations by Wang and Dolg [37] than Guido and Balducci [38]. For example, the error is 3.3% for the R_e of $B^1\Pi_u$ state corresponding to the result. The values (2.5509 eV and 49.1833 cm^{-1}) of electronic transition energy (T_e) and harmonic frequency (ω_e) of $A^1\Sigma_u^+$ are very close to the determinations (2.53 eV and 53 cm^{-1}) by Wang, respectively. In addition, we also provided anharmonic vibrational frequency $(\omega_e x_e)$ and rotational frequency (B_e) of five states first time. It indicates that using icMRCI + Q method and the larger basis set are important for studying PEC. That is to say, the PEC at icMRCI + Q/ECP60MDF/32213220 level is more accurate at present, which can be used to predict the spectral parameters of higher vibrational bands for every allowed transition system. Therefore, we will apply those potentials to investigate the Franck–Condon factors (FCFs) and Einstein A coefficients in Section 3.2.

While calculating the potential energy functions, the transition dipole moment curves (TDMCs) of the allowed transitions are also investigated in theory shown in 2, which included $A^1\Sigma_u^+ \longleftarrow X^1\Sigma_g^+$, $B^1\Pi_u \longleftarrow X^1\Sigma_g^+$, $C^1\Sigma_u^+ \longleftarrow X^1\Sigma_g^+$, and $D^1\Pi_u \longleftarrow X^1\Sigma_g^+$. It can be seen that the TDMCs of $A^1\Sigma_u^+ \longleftarrow X^1\Sigma_g^+$ and $C^1\Sigma_u^+ \longleftarrow X^1\Sigma_g^+$ firstly increase, but then $C^1\Sigma_u^+ \longleftarrow X^1\Sigma_g$ decreases until it approaches zero. On the contrary, the TDMs of $B^1\Pi_u \longleftarrow X^1\Sigma_g^+$ and
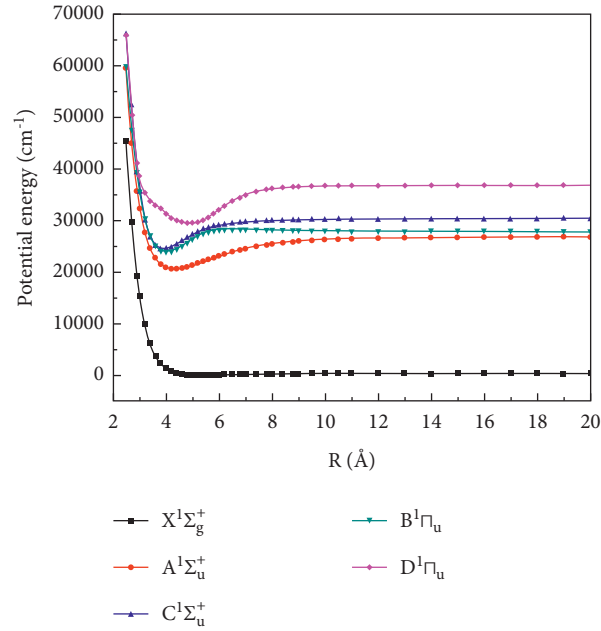
FIGURE 1: The calculated potential energy curves (PECs) at the icMRCI + Q/ECP60MDF/32213220 level.

TABLE 1: The spectroscopic parameters of calculated and experimental values of Yb_2.

States	R_e (A)	T_e (eV)	D_e (eV)	ω_e (cm^{-1})	$\omega_e\chi_e$ (cm^{-1})	B_e (cm^{-1})	Reference
	5.1120	0	0.0432	15.4967	0.2179	0.0075	This work
$X^1\Sigma_g^+$	5.158	0	0.041	15			[a]
	4.19	0	0.17	33			[c]
$A^1\Sigma_u^+$	4.2110	2.5509	0.7701	49.1833	0.0130	0.0105	This work
	3.894	2.53	0.97	53			[b]
$B^1\Pi_u$	4.0330	2.9670	0.5337	68.23261	0.3213	0.0120	This work
	3.873	3.26	0.62	68			[b]
$C^1\Sigma_u^+$	3.9180	3.0442	0.7301	63.4918	0.0071	0.01277	This work
$D^1\Pi_u$	4.9240	3.6675	0.8963	36.4166	0.0985	0.0080	This work

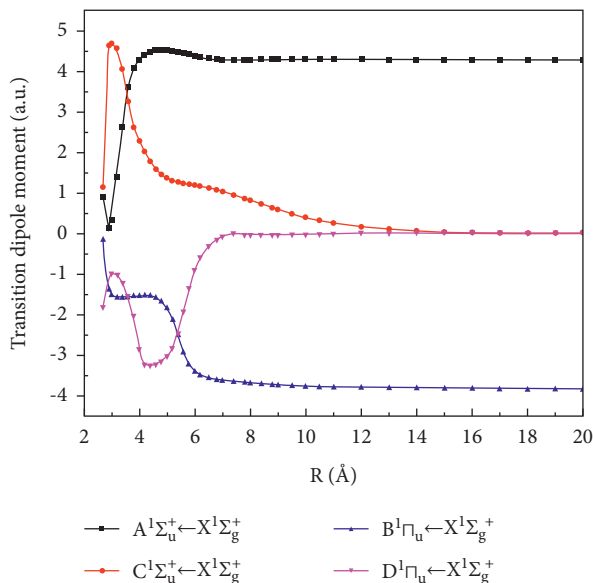[a]Yixuan Wang, Michael Dolg, 1998, CCSD; [b]used MRCI method; [c]Guido M, Balducci G., 1972.

FIGURE 2: Transition dipole moment curves for allowed transition of Yb_2 investigated in theory.

$D^1\Pi_u\longleftarrow X^1\Sigma_g^+$ decrease with R, and then the curve of $D^1\Pi_u\longleftarrow X^1\Sigma_g^+$ increases until it tends to zero. At the equipment internuclear distance of ground state, the values of TDMs are $A^1\Sigma_u^+\longleftarrow X^1\Sigma_g^+$: 4.51 a.u., $B^1\Pi_u\longleftarrow X^1\Sigma_g^+$: −1.84 a.u., $C^1\Sigma_u^+\longleftarrow X^1\Sigma_g^+$: 1.36 a.u., and $D^1\Pi_u\longleftarrow X^1\Sigma_g^+$: −3.04 a.u., respectively. At last, the molecule dissociated into two atoms with the R increase that lead the dipole moment to be a constant, which is regarded as polar compensation of each other. The reason for this situation is that the different polarity of two states ($A^1\Sigma_u^+$, $B^1\Pi_u$) at larger position tends to maximum (4.2 a.u. and 3.8 a.u., respectively). At the same time, the results of the TDMs of electronic states ($C^1\Sigma_u^+$, $D^1\Pi_u$) tend to zero.

3.2. Optical Transition Properties. Simulation of laser conversion of photoassociation requires systematic calculations of optical transition characteristics taking into account laser absorption from ground state to vibrational level of excited state [39]. By using LEVEL [36], the FCFs and vibrational transition probabilities have been calculated for quasi target

states of exited states. Firstly, we calculated the larger FCFs of every system corresponding to vibrational bands of the allowed transitions, shown in 3. It can be seen that FCFs of vibrational transitions of $A^1\Sigma_u^+ \leftarrow X^1\Sigma_g^+$ and $D^1\Pi_u \leftarrow X^1\Sigma_g^+$ are relatively larger than $B^1\Pi_u \leftarrow X^1\Sigma_g^+$ and $C^1\Sigma_u^+ \leftarrow X^1\Sigma_g^+$. The largest values of every state are $A^1\Sigma_u^+$: 0.083, $B^1\Pi_u$: 0.059, $C^1\Sigma_u^+$: 0.067, and $D^1\Pi_u$: 0.27, which correspond to upper-level $v' = 23, 50, 55$, and 0, respectively. For $D^1\Pi_u \leftarrow X^1\Sigma_g^+$ system, the FCF is much larger with respect to $A^1\Sigma_u^+ \leftarrow X^1\Sigma_g^+$. On this basis, Einstein A coefficients and lifetime will be conveniently expressed by the FCF results.

The Einstein A coefficients (also called vibrational transition probabilities) of transitional systems are investigated by combining potential energy with transition dipole moment at icMRCI/ECP60MDF/32213220 level. These transition probabilities $A_{v'v''}$, which are defined with equation $A_{v'J'v''J''} = 3.136189 \times 10^{-7} (S(J', J'')/2J' + 1)v_{v'J'v''J''}^3 |\langle \Psi_{v_jJ_j}(r)|M(r)|\psi_{v''J''}\rangle|^2$, have been calculated including main transition bands. The larger probabilities are located in the Frank-Condon region, and the largest value corresponds to a strong transition. The results of transitional systems are that $A^1\Sigma_u^+ \leftarrow X^1\Sigma_g^+$:$1.07 \times 10^7\,s^{-1}$, $B^1\Pi_u \leftarrow X^1\Sigma_g^+$: $3.18 \times 10^6\,s^{-1}$, $C^1\Sigma_u^+ \leftarrow X^1\Sigma_g^+$:$1.60 \times 10^6\,s^{-1}$, and $D^1\Pi_u \leftarrow X^1\Sigma_g^+$: $4.32 \times 10^7\,s^{-1}$ correspond to $v' = 23, 50, 55$, and 0 level, respectively.

According to Franck–Condon filtering and transitional probability, we plotted the selected vibrational levels v' of excited states with the population after photoassociation shown in 4, which provided a visualized description for the quantum control of photoassociation of Yb$_2$. The equilibrium internuclear distance of $D^1\Pi_u$ state is larger than $A^1\Sigma_u^+$ state that is similar to $B^1\Pi_u$ and $C^1\Sigma_u^+$. The ground $X^1\Sigma_g^+$ state is only weakly bound by van der Waals force and has larger equilibrium internuclear distance corresponding to the excited states. There is rotational barrier of $X^1\Sigma_g^+$ for rotational quantum numbers (J''), already for 218, where the ground states do not support any bound levels. Above all, $A^1\Sigma_u^+$ and $D^1\Pi_u$ are more suitable for the target states of photoassociation of Yb$_2$ molecule.

3.3. Dynamic Process of Selective Control for Photoassociation.

The associative process happens at short internuclear distance when a pair of colliding atoms are irradiated by a laser pulse. For selective control of photoassociation of Yb$_2$, the quantitative yield and purity of target states after association are concerned. By using quantum wave packet dynamics with time-dependent potentials [34], we calculated the projections with time evolution of photoassociation. The projections of time-dependent wave functions of initial states on the target vibrational eigenstates, reflecting the photoassociative yields of Yb$_2$, are investigated. In the calculations, the number of grid points is 4000, and the size of grid used was 0.02 a.u. We run the simulation with time 800000 a.u. and time step length $\Delta t = 0.1$ a.u. The projection of the wave function on vibrational eigenstates every 20000 time steps is printed. It happens that the population transfers from ground state to excited state after a pulse irradiance. In
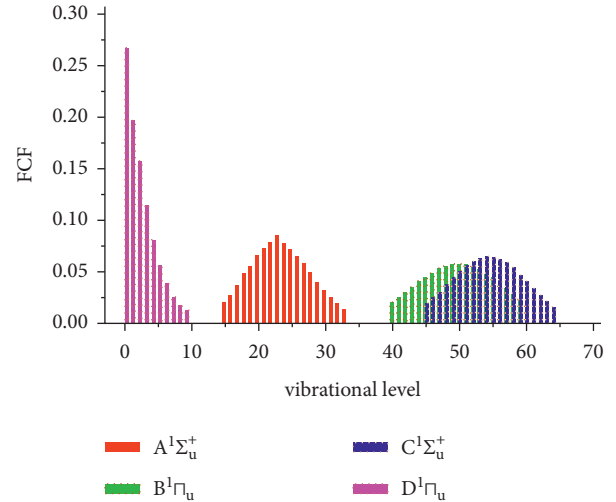

FIGURE 3: The Frank–Condon factors of transitions from the ground state to vibrational levels of excited states.
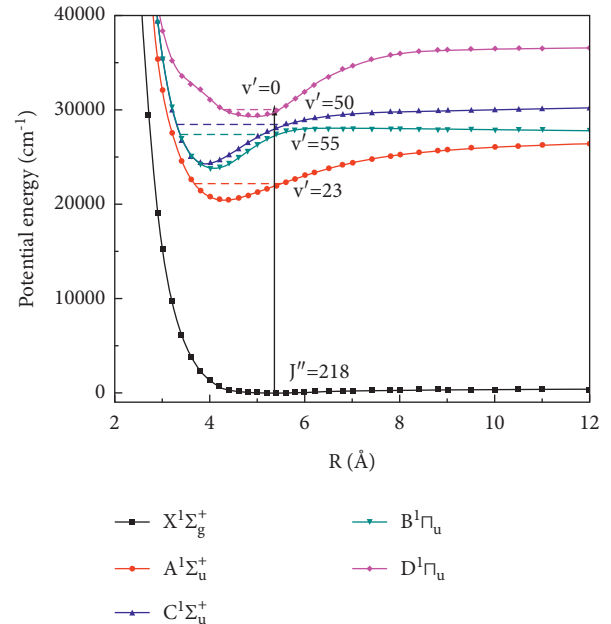

FIGURE 4: The selected optimally vibrational target states of excited states of Yb$_2$.

this work, the initial population is defined as 100% of ground $X^1\Sigma_g^+$ of Yb$_2$.

In 555 5, the projections of time-dependent vibrational wave function of ground state, interacting with a resonant laser pulse, on the main five vibrational eigenstates of excited states ($A^1\Sigma_u^+, B^1\Pi_u, C^1\Sigma_u^+, D^1\Pi_u$) are plotted. That corresponds to laser pulse parameters: amplitude $\varepsilon_0 = 0.169$ a.u.; duration $t_f = 41341.37$ a.u.; frequency ω match transition energy. From 5, it can be seen that, with the time evolution, the percent of yields for every state is about $A^1\Sigma_u^+$: 13%, $B^1\Pi_u$: 8%, $C^1\Sigma_u^+$: 9%, and $D^1\Pi_u$: 70%, respectively. Meanwhile, the corresponding yield of each state firstly increases and then decreases with time evaluation. But, when each state reaches the maximum yield, the
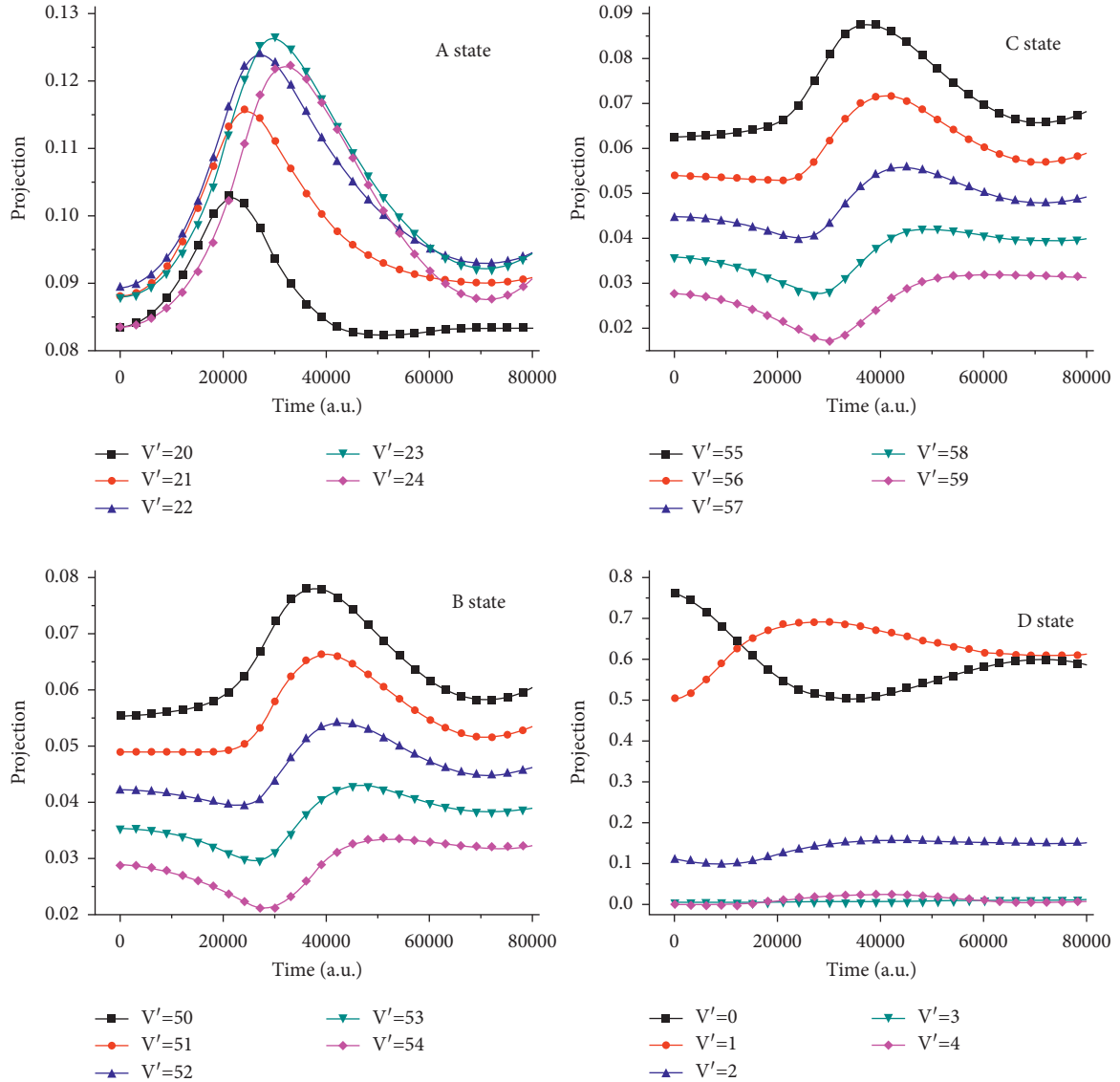
FIGURE 5: The projections of the time-dependent vibrational wave function of Yb$_2$, interacting with a resonant laser pulse, on the main five vibrational eigenstates of excited states ($A^1\Sigma_u^+$, $B^1\Pi_u$, $C^1\Sigma_u^+$, and $D^1\Pi_u$), corresponding to laser pulse parameters: amplitude $\varepsilon_0 = 0.169$; duration $t_f 41341.37$; frequency ω matches transition energy (in atomic units).

needed time is different, which is $A^1\Sigma_u^+$ ($v' = 23$): 30000 a.u., $B^1\Pi_u$ (v' 50): 36000 a.u., $C^1\Sigma_u^+$ (v' 55): 39000 a.u., and $D^1\Pi_u$ (v' 1): 27000 a.u., respectively. In addition, when every vibrational energy level reaches the maximum, the required time becomes longer with the level. This indicates that the probability of optical transition of $A^1\Sigma_u^+$ state is greater than $B^1\Sigma_u^+$ and $C^1\Sigma_u^+$ states, which is just different from $D^1\Pi_u$. This conclusion is the same as that discussed above that the optimal target states of photoassociation are $A^1\Sigma_u^+$ state and $D^1\Pi_u$ state. The proposed laser drive transitions to target states of photoassociative process at wavelength $A^1\Sigma_u^+$: 464.7 nm, $B^1\Pi_u$: 373.1 nm, $C^1\Sigma_u^+$: 361.8 nm, and $D^1\Pi_u$: 339.1 nm are obtained.

For quasi target state $A^1\Sigma_u^+$ of photoassociation, the projections of initial wave function on the five vibrational eigenstates (v' 20–24) are investigated, and the results are shown in 6. At the initial time, the projections of each vibrational state are similar about 66%. By changing the laser intensity and pulse shape, we have studied the effects on yield and purity of photoassociative process. When laser intensity changed from 0.169 to 1.69 a.u. (equivalent to 1.0×10^{14} W/cm^2), the yield of association was improved. For example, using Gaussian pulse made the value of v' 23 up to 96% at 725 fs. Furthermore, by changing the shapes of laser pulse, the developed trend of yield over time had been evaluated according to Figure 6 of ±chirp pulse. From the figure, it can be seen that, after a laser pulse, the positive chirp makes the projections of vibrational states increase, but the negative chirp makes it decrease. When the intensity of chirp pulse increases to 1.0×10^{14} W/cm^2, the yield of v' 24 is larger than other vibrational levels (v' 20, 21, 22, 23), in which the value reached maximum 99%. It is contrary to the result of Gaussian shape. Meanwhile, the needed time of the maximum yield will be shorter by using chirp pulse. Even the
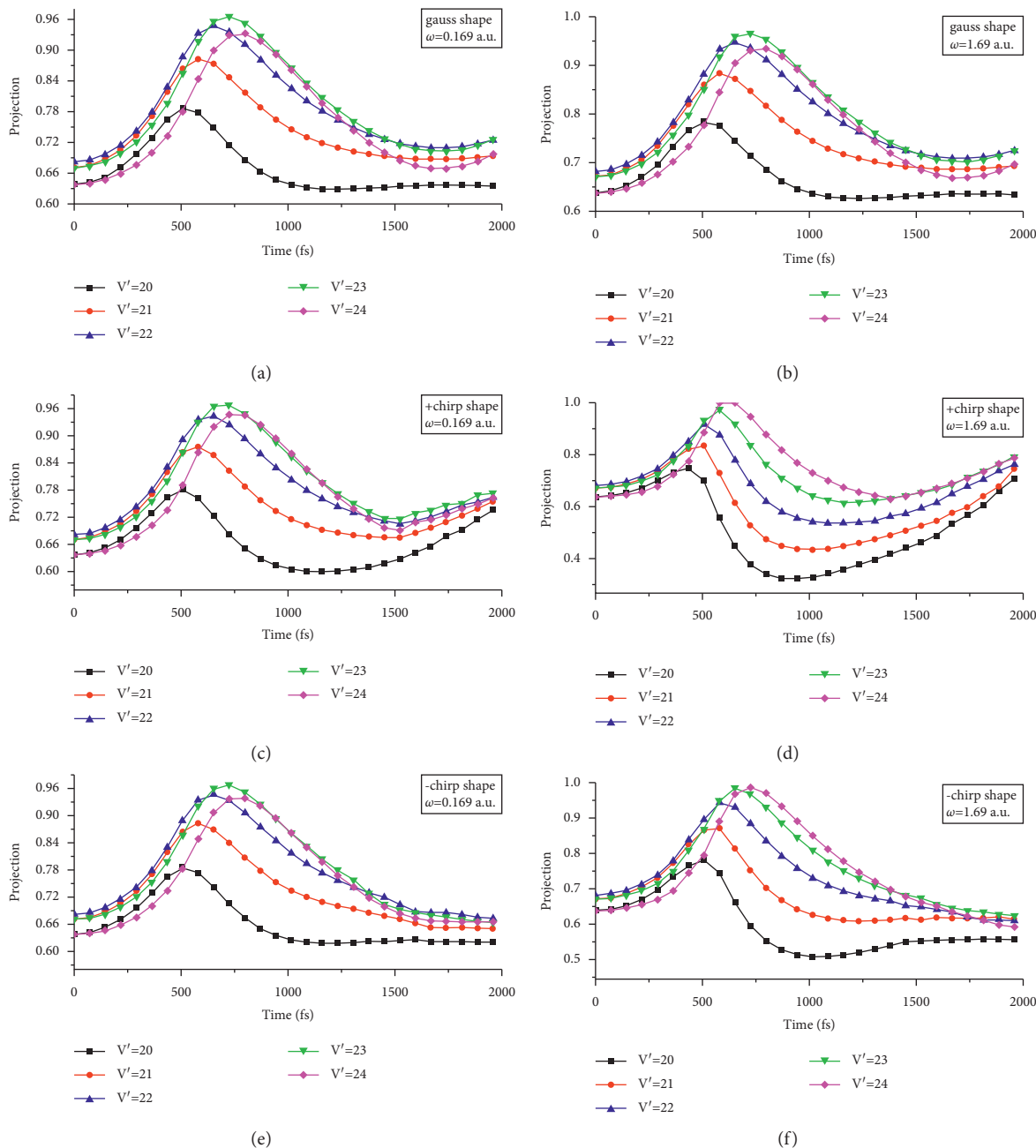
(a)

(b)

(c)

(d)

(e)

(f)

FIGURE 6: The effect on the projection of the $A^1\Sigma_u^+$ state by changing pulse shapes and laser intensities: (a, b) Gaussian profile; (c, d) +chirp profile; (e, f) −chirp profile.

result by positive chirp (580 fs) is much shorter than negative chirp (653 fs). That is to say, the positive chirp pulse could effectively promote the yields of photochemical reactions, and negative chirp could inhibit them. In addition, it indicates that the purity is not very well due to the overlap of projections. Therefore, the yields of vibrational levels are relatively lower. That do not benefit our accurate quantum manipulation of photoassociation.

We came to the same conclusion with above: at initial time (t 0 fs), the selected optimal vibrational target state is v' 0 for target $D^1\Pi_u$ of photoassociation, shown in 7. There is a diverse oscillatory behavior observed from Figure 7(a). The

reason for this behavior is that the optical target states correspond to some frequencies of vibrational wave functions. So, they lead to the diverse overlap of two wave functions of v'0 and v'1. The projections of five vibrational levels before 750 fs are overlap, so that we are difficult to distinguish which one is optimal vibrational target state for photoassociation. When laser intensity is 1.0×10^{14} W/cm^2, not only the purity but also the yield is higher up to 99% of target state v'0 at 1570 fs in Figure 7(c). By changing the laser intensity into 1.69 a.u. of negative chirp in Figure 7(e), the excess energy was absorbed by other vibrational levels except v' 1, which lead to a little increase for the yields of v' 2, 3, and
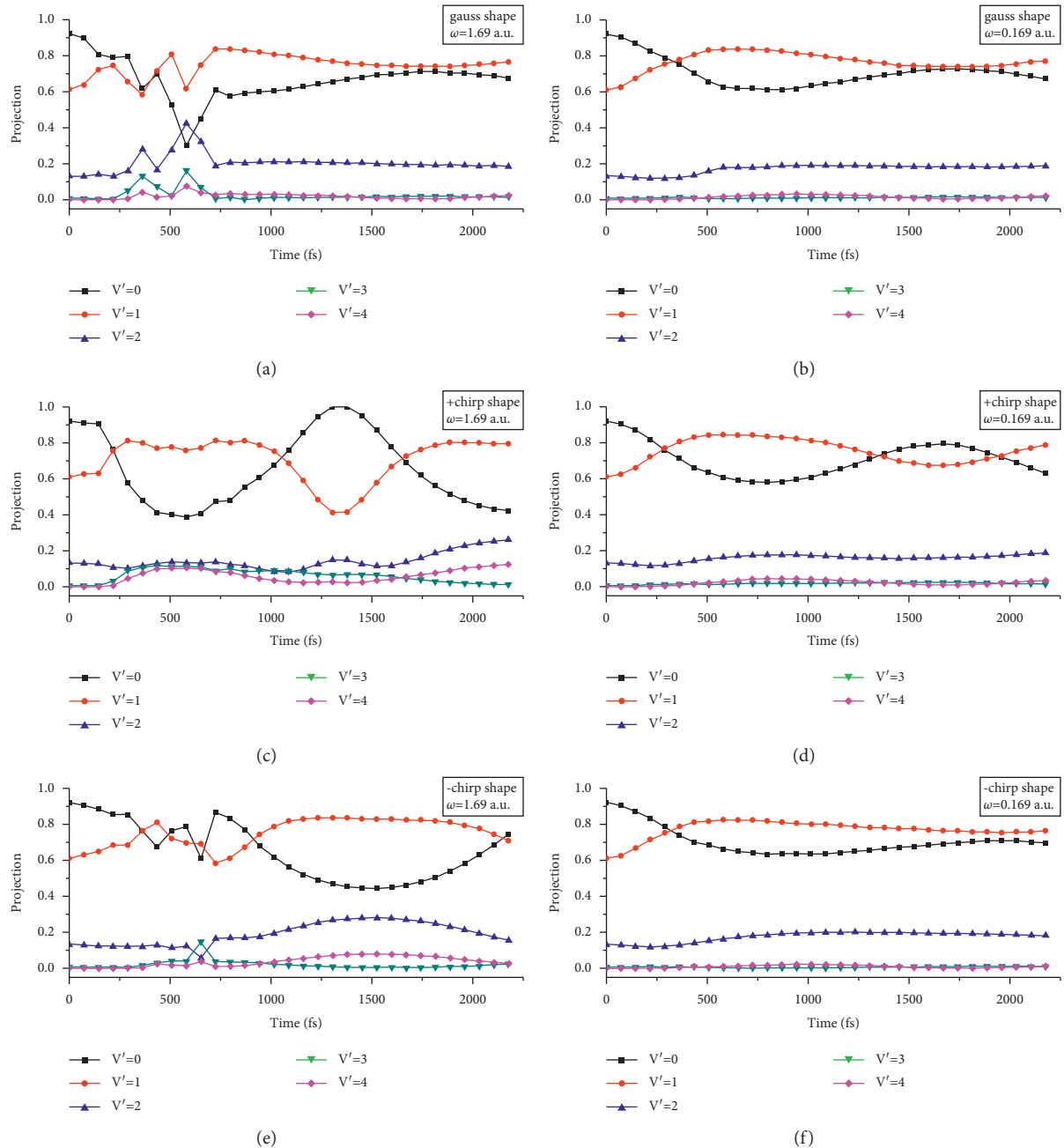
FIGURE 7: The effect on the projection of the $D^1\Pi_u$ state by changing pulse shapes and laser intensities: (a, b) Gauss pulse; (c, d) +chirp pulse; (e, f) −chirp pulse.

4. In other words, the purity of target state had a sudden drop and then levels off at longer duration when increasing laser intensity. Generally, the projection of time-dependent vibrational wave function recovers the prior level after a pulse. However, the case of $D^1\Pi_u$ shows a little change, which is a change between v' 0 and v' 1. The reason is that the excess energy of v' 0 after pulse was absorbed by v' 1, leading to the final population having a little increase of v' 1, 2, 3, and 4. But the finally total population keeps the same level with initial population. The calculated yield of photoassociation is further enhanced by performing optimization of the best laser pulse.

On the whole, for Yb_2 molecule, if the photoassociative process is nonadiabatic, the yields of target states are $A^1\Sigma_u^+$: 0.13%, $B^1\Pi_u$: 0.08%, $C^1\Sigma_u^+$: 0.09%, and $D^1\Pi_u$: 0.70%, respectively. If we use adiabatic association, the most suitable quantum manipulation of photoassociation is $A^1\Sigma_u^+$ and $D^1\Pi_u$ states that correspond to photoassociative yields are 67% and 89% at initial time by Gaussian pulse. We also evaluated the projections interacting with positive and negative chirp laser pulse, which show that the yields of vibrational states have an increase and decrease of a little after the pulse, respectively. That is to say, different chirp pulses can be used to effectively promote or inhibit the yields

of photochemical reactions. Therefore, it could much more easily control the photochemical along our desired direction by changing the pulse shape. It was found that both high yield and high purity of femtosecond photoassociation of Yb_2 molecule correspond to an optimal laser pulse with intensity 1.0×10^{14} W/cm^2, duration 1350 fs, and frequency 29290 cm^{-1} by positive chirp. The maximum photoassociative yield is up to 99% of optimal target $D^1\Pi_u$ state for selected level v' 0. Those conditions are the best situation for quantum selective control of photoassociation.

4. Conclusions

In this work, the potential energy curves and transition dipole moment function for excited states of Yb_2 were calculated based on CASSCF/icMRCI + Q method with ECP60MDF basis set and 32213220 active spaces. The spectroscopic constants of PECs for five states are in good agreement with the experimental determinations. Combining the PECs with TDMCs, the optical transitional characters are investigated including Franck–Condon factors and Einstein A coefficients. By Franck–Condon filtering, the selective control of laser synthesis of Yb_2 molecule is achieved by purification. The corresponding vibrational transition levels from $X^1\Sigma_g^+$ to excited state ($A^1\Sigma_u^+$, $B^1\Pi_u$, $C^1\Sigma_u^+$, $D^1\Pi_u$) are v' 23, 50, 55, and 0, respectively. The laser drive transitions to target states of association at wavelengths $A^1\Sigma_u^+$: 464.7 nm, $B^1\Pi_u$: 373.1 nm, $C^1\Sigma_u^+$: 361.8 nm, and $D^1\Pi_u$: 339.1 nm are obtained.

Based on the transitional properties, the corresponding associative yield and purity of photoassociative process have been calculated by using quantum wave packet dynamic method. The target states of photoassociation are $A^1\Sigma_u^+$ state and $D^1\Pi_u$ state. For $A^1\Sigma_u^+$, it is indicated that using Gaussian pulse made the value of v' 23 up to 97% at 725 fs. After a laser pulse, the positive chirp promotes the yield of vibrational states to increase, but the negative chirp inhibits it. For $D^1\Pi_u$, when laser intensity is 1.0×10^{14} W/cm^2, not only the purity but also the yield is higher up to 99% for target state $v' = 0$ at 1350 fs. That is to say, by changing the laser parameters and pulse shapes, it could more easily control the photochemical reaction along our desired direction. Those conditions will provide an important reference and suggest a scheme for a feasible photoassociation for further experimental and theoretical researches. A feasible route to the control of photo-induced bimolecular chemical reactions will come true. Current study also may promote an important step toward the realization of highly accurate quantum manipulation and control of binary photoreactions.

Data Availability

All data that support the findings of this study are included within the article.

Conflicts of Interest

The authors declare no conflicts of interest.

References

[1] H. Katori, "Optical lattice clocks and quantum metrology," *Nature Photonics*, vol. 5, no. 4, 203 pages, 2011.

[2] A. D. Ludlow, M. M. Boyd, J. Ye, E. Peik, and P. O. Schmidt, "Optical atomic clocks," *Reviews of Modern Physics*, vol. 87, no. 2, 637 pages, 2015.

[3] C. W. Chou, D. B. Hume, T. Rosenband, and D. J. Wineland, "Optical clocks and relativity," *Science*, vol. 329, no. 5999, 1630 pages, 2010.

[4] T. M. Fortier, N. Ashby, J. C. Bergquist et al., "Precision atomic spectroscopy for improved limits on variation of the fine structure constant and local position invariance," *Physical Review Letters*, vol. 98, Article ID 070801, 2007.

[5] S. Blatt, A. D. Ludlow, G. K. Campbell et al., "New limits on coupling of fundamental constants to gravity using ^{87}Sr optical lattice clocks," *Physical Review Letters*, vol. 100, Article ID 140801, 2008.

[6] C. Orzel, "Searching for new physics through atomic, molecular and optical precision measurements," *Physica Scripta*, vol. 86, Article ID 068101, 2012.

[7] M. J. Martin, M. Bishof, M. D. Swallows et al., "A quantum many-body spin system in an optical lattice clock," *Science*, vol. 341, no. 6146, 632 pages, 2013.

[8] A. Dareau, M. Scholl, Q. Beaufils, D. Döring, J. Beugnon, and F. Gerbier, "Doppler spectroscopy of an ytterbium BoseEinstein condensate on the clock transition," *Physical Review A*, vol. 91, Article ID 023626, 2015.

[9] A. Derevianko and M. Pospelov, "Hunting for topological dark matter with atomic clocks," *Nature Physics*, vol. 10, no. 12, 933 pages, 2014.

[10] P. Wcis ło, P. Morzyński, M. Bober et al., "Experimental constraint on dark matter detection with optical atomic clocks," *Nature Astronomy*, vol. 1, 2016.

[11] A. Shelkovnikov, R. J. Butcher, C. Chardonnet, and A. Amy-Klein, "Stability of the proton-to-electron mass ratio," *Physical Review Letters*, vol. 100, Article ID 150801, 2008.

[12] T. Zelevinsky, S. Kotochigova, and J. Ye, "Precision test of mass-ratio variations with lattice-confined ultracold molecules," *Physical Review Letters*, vol. 100, Article ID 043201, 2008.

[13] D. Demille, S. Sainis, J. Sage, T. Bergeman, S. Kotochigova, and E. Tiesinga, "Enhanced sensitivity to variation of me/mp in molecular spectra," *Physical Review Letters*, vol. 100, Article ID 043202, 2008.

[14] K. Beloy, A. W. Hauser, A. Borschevsky, V. V. Flambaum, and P. Schwerdtfeger, "Effect of α variation on the vibrational spectrum of Sr_2," *Physical Review A*, vol. 84, Article ID 062114, 2011.

[15] M. Borkowski, "Optical lattice clocks with weakly bound molecules," *Physica Scripta*, vol. 120, Article ID 083202, 2018.

[16] M. Borkowski, R. Ciurylo, and P. S. Julienne, "Photoassociative production of ultracold heteronuclear ytterbium molecules," *Physical Review A*, vol. 84, Article ID 030702, 2011.

[17] S. Origlia, "A high-performance optical lattice clock based on bosonic atoms," *Physical Review A*, vol. 98, Article ID 053443, 2018.

[18] C. Radzewicz, "Accuracy budget of the 88Sr optical atomic clocks at KL FAMO," *Physica Scripta*, vol. 91, Article ID 084003, 2016.

[19] M. Borkowski, "Mass scaling and nonadiabatic effects in photoassociation spectroscopy," *Physical Review A*, vol. 90, Article ID 032713, 2014.

[20] W. Skomorowski, F. Pawłowski, C. P. Koch, and R. Moszynski, "Rovibrational dynamics of the strontium molecule in the AΣu+1, c3Πu, and aΣu+3 manifold from state-of-the-art ab initio calculations," *The Journal of Chemical Physics*, vol. 136, no. 19, Article ID 194306, 2012.

[21] L. Franchi, L. F. Livi, G. Cappellini et al., "State-dependent interactions in ultracold174Yb probed by optical clock spectroscopy," *New Journal of Physics*, vol. 19, no. 10, Article ID 103037, 2017.

[22] M. Bober, M. Borkowski, P. Morzynski et al., "Photoassociation measurements to evaluate collisional shifts in strontium and prospects for clock spectroscopy with ytterbium molecules," *Physical Review Letters*, vol. 326, 2018.

[23] J. H. Han, H. Jin, M. Lee, and Y. Shin, "Photoassociation spectroscopy of ultracold [173]Yb atoms near the intercombination line," *Physical Review A*, vol. 97, Article ID 013401, 2018.

[24] T. Urbanczyk, M. Strojecki, and J. Koperski, "Exploration of the molecular ro-vibrational energy structure: on the perspective of Yb and Cd internal cooling, and Yb-version of Einstein–Podolsky–Rosen experiment," *Molecular Physics*, vol. 143, pp. 1–12, 2018.

[25] R. Roy, R. Shrestha, A. Green, and S. Gupta, "Photoassociative production of ultracold heteronuclear YbLi molecules," *Physical Review A*, vol. 94, Article ID 033413, 2016.

[26] M. B. Shundalau and A. A. Minko, "Ab initio multi-reference perturbation theory calculations of the ground and some excited electronic states of the RbYb molecule," *Physica Scripta*, vol. 1103, pp. 11–16, 2017.

[27] S. Kotochigova, A. Petrov, M. Linnik, J. Kłos, and P. S. Julienne, "Ab initio properties of Li-group-II molecules for ultracold matter studies," *The Journal of Chemical Physics*, vol. 135, no. 16, Article ID 164108, 2011.

[28] H. J. Werner, P. J. Knowles, R. Lindh et al., "MOLPRO Is a Package of Ab Initio Programs," 2009, http://www.molpro.net.

[29] P. J. Knowles and H.-J. Werner, "An efficient second-order MC SCF method for long configuration expansions," *Chemical Physics Letters*, vol. 115, no. 3, pp. 259–267, 1985.

[30] H. J. Werner and P. J. Knowles, "A second order multi-configuration SCF procedure with optimum convergence," *The Journal of Chemical Physics*, vol. 82, no. 11, pp. 5053–5063, 1985.

[31] S. R. Laughoff and E. R. Davidson, "Configuration interaction calculations on the nitrogen molecule," *International Journal of Quantum Chemistry*, vol. 8, pp. 61–72, 1974.

[32] M. Dolg and X. Cao, "Relativistic pseudopotentials: their development and scope of applications," *Chemical Reviews*, vol. 112, no. 1, pp. 403–480, 2012.

[33] R. A. Carollo, J. L. Carini, E. E. Eyler, P. L. Gould, and W. C. Stwalley, "Short-range photoassociation from the inner wall of the lowest triplet potential of85Rb2," *Journal of Physics B: Atomic, Molecular and Optical Physics*, vol. 49, no. 19, 194001 pages, 2016.

[34] C. M. Dion, A. Hashemloo, and G. Rahali, "Program for quantum wave-packet dynamics with time-dependent potentials," *Computer Physics Communications*, vol. 185, no. 1, pp. 407–414, 2014.

[35] J. X. Cheng, H. Zhang, X. L. Cheng, and S. J. Wu, "Selective control of photoassociation of alkaline earth dimers: a theoretical study," *International Journal of Quantum Chemistry*, vol. 26027, pp. 1–14, 2019.

[36] R. J. Le Roy, "LEVEL 8.0, a computer program for solving the radial Schrodinger equation for bound and quasibound levels," *Chemical Physics Research Report*, Vol. 663, University of Waterloo, Waterloo, ON, USA, 2007.

[37] Y. Wang and M. Dolg, "Pseudopotential study of the ground and excited states of Yb 2," *Theoretical Chemistry Accounts: Theory, Computation, and Modeling*, vol. 100, no. 1–4, pp. 124–133, 1998.

[38] M. Guido and G. Balducci, "Dissociation energy of Yb2," *The Journal of Chemical Physics*, vol. 57, no. 12, 5611 pages, 1972.

[39] E. A. Pazyuk, A. V. Zaitsevskii, A. V. Stolyarov, M. Tamanis, and R. Ferber, "Laser synthesis of ultracold alkali metal dimers: optimization and control," *Russian Chemical Reviews*, vol. 84, no. 10, pp. 1001–1020, 2015.